Proceedings of the
47th IEEE Conference on Decision and Control
Cancun, Mexico, Dec. 9-11, 2008

Input-output analysis of the 2D/3C model in channel flows of viscoelastic fluids

Nazish Hoda, Mihailo R. Jovanović, and Satish Kumar

Abstract— **Energy amplification in streamwise constant channel flows of viscoelastic fluids is studied from an input-output point of view by analyzing the responses of the velocity components to spatio-temporal body forces. These inputs into governing equations are assumed to be harmonic in spanwise direction and stochastic in the wall-normal direction and in time. An explicit Reynolds number scaling of frequency responses from different input to different output components is developed. It is found that some of the components of frequency response peak at nonzero temporal frequencies. This is in contrast to the Newtonian fluids, where peaks are always observed at zero frequency, suggesting that viscoelastic effects introduce additional timescales and promote development of flow patterns with smaller time constants than in Newtonian fluids. The frequencies, corresponding to the peaks in the components of frequency response, decrease with an increase in viscosity ratio and show maximum for non-zero elasticity number. At low Reynolds numbers, the energy density decreases monotonically when the elasticity number is sufficiently small, but shows a maximum when the elasticity number becomes sufficiently large, suggesting that elasticity can amplify disturbances even when inertial effects are weak.**

Index Terms— **Input-output analysis, viscoelastic fluids, transition to turbulence, Reynolds-number scaling.**

I. Introduction

The inception and evolution of amplification of disturbances in viscoelastic fluid flows is an active area of research due to the rich physical interactions present in and the enormous practical importance of such flows. Even for the seemingly simple cases of channel flows, understanding of the conditions under which transition to turbulence occurs remains far less complete relative to that for Newtonian fluids [1]. For channel flows of Newtonian fluids, it is by now widely recognized that standard linear stability analysis can be misleading due to the non-normal nature of the dynamical generator in the linear stability problem [2]. Linear dynamical systems with non-normal generators can have solutions that grow substantially transiently, even though they decay asymptotically. This so-called transient growth is generally overlooked in standard linear stability analysis (which typically focuses only on the least stable eigenvalues), and could put the system into a regime where nonlinear interactions are no longer negligible. The same issue will arise for viscoelastic fluids, making it important to investigate non-modal phenomena in these flows as well.

N. Hoda and S. Kumar are with the Department of Chemical Engineering and Materials Science, University of Minnesota, Minneapolis, MN 55455, USA (hoda@cems.umn.edu, kumar@cems.umn.edu). Partially supported by the Donors of The American Chemical Society Petroleum Research Fund.

M. R. Jovanović is with the Department of Electrical and Computer Engineering, University of Minnesota, Minneapolis, MN 55455, USA (mihailo@umn.edu). Partially supported by the National Science Foundation under CAREER Award CMMI-06-44793.

This study complements a previous study by the authors [3], where the aggregate effect of disturbances was examined, and helps in understanding the relative importance of the disturbances on the different velocity components for streamwise constant fluctuations. Because Ref. [3] focused on aggregate effects, as parameterized by the H_2 norm, it leaves open the question of exactly which velocity components are most amplified and which forcing components are responsible for this amplification. Furthermore, since the H_2 norm is a time-integrated quantity, it does not yield information about most amplified temporal frequencies. The present work addresses these issues and provides some explicit scaling relationships.

Our presentation is organized as follows: in § II, a model for streamwise constant channel flows of viscoelastic fluids with forcing is presented. In § III, a brief summary of a notion of the spatio-temporal frequency response is provided. In § IV, an explicit scaling of the components of frequency response with the Reynolds number is given. In § V and § VI, the effects of elasticity number and viscosity ratio on the different components of frequency response are studied. Finally the important findings are summarized in § VII.

II. The cross sectional 2D/3C model

We analyze the dynamical properties of the governing equations, for an Oldroyd-B fluid [4], with spatially distributed and temporally varying body force fields. The parameters characterizing Oldroyd-B fluids are: (a) the viscosity ratio, $\beta = \eta_s/(\eta_s + \eta_p)$, where η_s and η_p are the solvent and polymer viscosities, respectively; (b) the Reynolds number, $Re = U_o L/\nu = \rho U_o L/(\eta_s + \eta_p)$, which represents the ratio of inertial and viscous forces, where ρ denotes fluid's density; (c) the Weissenberg number, $We = \lambda U_o/L$, which characterizes the importance of the fluid relaxation time, λ, and the characteristic flow time, L/U_o. Another important parameter is the elasticity number, $\mu = We/Re = \lambda\nu/L^2$, which quantifies the ratio between the fluid relaxation time, λ, and the vorticity diffusion time, L^2/ν.

In this paper, we confine our analysis to the streamwise constant perturbations. In this special case, the model for flow perturbations is usually referred to as the two-dimensional, three component (2D/3C) model [5]. (2D indicates that dynamics evolve in cross sectional (y, z)-plane, and 3C indicates that velocity components in all three spatial directions are considered.) The motivation for a thorough analysis of this particular model is twofold: (a) a recent study by the authors suggests that the streamwise constant perturbations in channel flows of Oldroyd-B fluids create the largest contribution to kinetic energy density [3]; and (b) for 2D/3C model, an explicit Re-dependence for the components of the frequency response can be obtained,

978-1-4244-3124-3/08/$25.00 ©2008 IEEE

which clarifies the effectiveness (energy content) of forcing (velocity) components.

The dynamics of forced governing equations for streamwise constant ($k_x = 0$) perturbations are described by [3]

$$\begin{aligned} \boldsymbol{\psi}_t(y,k_z,t) &= \mathbf{A}(k_z)\boldsymbol{\psi}(y,k_z,t) + \bar{\mathbf{B}}(k_z)\mathbf{d}(y,k_z,t), \\ \mathbf{v}(y,k_z,t) &= \mathbf{C}(k_z)\boldsymbol{\psi}_1(y,k_z,t). \end{aligned} \tag{1}$$

Here, k_z is the spanwise wavenumber, $\boldsymbol{\psi} := \left[\begin{array}{cc} \boldsymbol{\psi}_1^T & \boldsymbol{\psi}_2^T \end{array}\right]^T$, $\boldsymbol{\psi}_1 := \left[\begin{array}{cc} v & \omega_y \end{array}\right]^T$, $\boldsymbol{\psi}_t := \partial_t\boldsymbol{\psi}$, with v and ω_y denoting the wall-normal velocity and vorticity, respectively. The components of polymer stresses are given by $\boldsymbol{\psi}_2 := \left[\begin{array}{cccccc} \tau_{xx} & \tau_{yy} & \tau_{zz} & \tau_{xy} & \tau_{xz} & \tau_{yz} \end{array}\right]^T$. A spatio-temporal body force is represented by $\mathbf{d}$, $\mathbf{d} := \left[\begin{array}{ccc} d_1 & d_2 & d_3 \end{array}\right]^T$, where d_1, d_2, and d_3 are the body forces in the streamwise (x), wall-normal (y), and spanwise (z) directions, respectively. These body forces are considered to be stochastic and they serve as inputs into the system of equations (1) that governs evolution of velocity and polymer stress fluctuations. Our objective is to investigate their effect on the components of the velocity field $\mathbf{v}$, $\mathbf{v} := \left[\begin{array}{ccc} u & v & w \end{array}\right]^T$.

The operator $\mathbf{A}$ in (1) is referred to as the dynamical generator of the linearized dynamics and it characterizes internal properties of the system (e.g., modal stability). The definition of this operator for full three-dimensional fluctuations is provided in [3]; the definition of components of this operator suitable for frequency response analysis of 2D/3C model is given in Eqs. (2) and (F) below. We also note that operator $\bar{\mathbf{B}}$ can be partitioned as $\bar{\mathbf{B}} = \left[\begin{array}{cc} \mathbf{B}^T & \mathbf{O}^T \end{array}\right]^T$, where $\mathbf{B}$ describes how forcing enters into the Orr-Sommerfeld and Squire equations of viscoelastic channel flows, and $\mathbf{O}$ is a 6×3 matrix of null operators. On the other hand, operator $\mathbf{C}$ in (1) contains information about a kinematic relationship between $\boldsymbol{\psi}_1$ and velocity fluctuation vector $\mathbf{v}$. These two operators are determined by:

$$\mathbf{B} = \left[\begin{array}{ccc} 0 & \mathbf{B}_2 & \mathbf{B}_3 \\ \mathbf{B}_1 & 0 & 0 \end{array}\right], \quad \mathbf{C} = \left[\begin{array}{cc} 0 & \mathbf{C}_u \\ \mathbf{C}_v & 0 \\ \mathbf{C}_w & 0 \end{array}\right],$$

$\{\mathbf{B}_1 = \mathrm{i}k_z,\ \mathbf{B}_2 = -k_z^2\boldsymbol{\Delta}^{-1},\ \mathbf{B}_3 = -\mathrm{i}k_z\boldsymbol{\Delta}^{-1}\partial_y\}$, $\{\mathbf{C}_u = -(\mathrm{i}/k_z),\ \mathbf{C}_v = \mathbf{I},\ \mathbf{C}_w = (\mathrm{i}/k_z)\partial_y\}$, where $\mathrm{i} := \sqrt{-1}$, $\boldsymbol{\Delta} := \partial_{yy} - k_z^2$ is Laplacian with Dirichlet boundary conditions, and $\boldsymbol{\Delta}^{-1}$ denotes the inverse of the Laplacian. System (1) is subject to the following boundary conditions: $\{v(\pm 1, k_z, t) = \partial_y v(\pm 1, k_z, t) = \omega_y(\pm 1, k_z, t) = 0\}$, that come from the no-slip and no-penetration prerequisites on the velocity components. We note that there are no constraints on the boundary conditions of the polymer stresses.

A coordinate transformation $\boldsymbol{\phi} = \mathbf{T}\boldsymbol{\psi}$ with $\{\phi_1 := v,\ \boldsymbol{\phi}_2 := \left[\begin{array}{ccc} \tau_{yy} & \tau_{yz} & \tau_{zz} \end{array}\right]^T,\ \phi_3 := \omega_y,\ \boldsymbol{\phi}_4 := \left[\begin{array}{cc} \tau_{xy} & \tau_{xz} \end{array}\right]^T,\ \phi_5 := \tau_{xx}\}$ can be used to bring system (1) into the following form:

$$\phi_{1t} = \frac{\beta}{Re}\,\mathbf{F}_{11}\,\phi_1 + \frac{1-\beta}{Re}\,\mathbf{F}_{12}\,\boldsymbol{\phi}_2 + \mathbf{B}_2\,d_2 + \mathbf{B}_3\,d_3, \tag{2a}$$

$$\boldsymbol{\phi}_{2t} = -\frac{1}{\mu Re}\,\boldsymbol{\phi}_2 + \frac{1}{\mu Re}\,\mathbf{F}_{21}\,\phi_1, \tag{2b}$$

$$\phi_{3t} = \frac{\beta}{Re}\,\mathbf{F}_{33}\,\phi_3 + \mathbf{F}_{31}\,\phi_1 + \frac{1-\beta}{Re}\,\mathbf{F}_{34}\,\boldsymbol{\phi}_4 + \mathbf{B}_1\,d_1, \tag{2c}$$

$$\boldsymbol{\phi}_{4t} = -\frac{1}{\mu Re}\,\boldsymbol{\phi}_4 + \mathbf{F}_{41}\,\phi_1 + \mathbf{F}_{42}\,\boldsymbol{\phi}_2 + \frac{1}{\mu Re}\,\mathbf{F}_{43}\,\phi_3, \tag{2d}$$

$$\phi_{5t} = -\frac{1}{\mu Re}\,\phi_5 - \mu Re\,\mathbf{F}_{51}\,\phi_1 + \mathbf{F}_{53}\,\phi_3 + \mathbf{F}_{54}\,\boldsymbol{\phi}_4, \tag{2e}$$

$$\left[\begin{array}{c} u \\ v \\ w \end{array}\right] = \left[\begin{array}{cc} 0 & \mathbf{C}_u \\ \mathbf{C}_v & 0 \\ \mathbf{C}_w & 0 \end{array}\right] \left[\begin{array}{c} \phi_1 \\ \phi_3 \end{array}\right], \tag{2f}$$

where the $\mathbf{F}$-operators are given by:

$$\begin{aligned} &\mathbf{F}_{11} = \boldsymbol{\Delta}^{-1}\boldsymbol{\Delta}^2, \quad \mathbf{F}_{33} = \boldsymbol{\Delta}, \quad \mathbf{F}_{31} = -\mathrm{i}k_z U'(y), \\ &\mathbf{F}_{12} = \boldsymbol{\Delta}^{-1}\left[\begin{array}{ccc} -k_z^2\partial_y & -\mathrm{i}k_z\left(\partial_{yy} + k_z^2\right) & k_z^2\partial_y \end{array}\right], \\ &\mathbf{F}_{34} = \left[\begin{array}{cc} \mathrm{i}k_z\partial_y & -k_z^2 \end{array}\right], \quad \mathbf{F}_{43} = -(1/k_z^2)\mathbf{F}_{34}^T, \\ &\mathbf{F}_{21} = \left[\begin{array}{ccc} 2\partial_y & (\mathrm{i}/k_z)\left(\partial_{yy} + k_z^2\right) & -2\partial_y \end{array}\right]^T, \\ &\mathbf{F}_{41} = \left[\begin{array}{c} U'(y)\partial_y - U''(y) \\ (\mathrm{i}/k_z)U'(y)\partial_{yy} \end{array}\right], \\ &\mathbf{F}_{42} = \left[\begin{array}{ccc} U'(y) & 0 & 0 \\ 0 & U'(y) & 0 \end{array}\right], \ \mathbf{F}_{51} = 4U'(y)U''(y), \\ &\mathbf{F}_{53} = -(2\mathrm{i}/k_z)U'(y)\partial_y, \quad \mathbf{F}_{54} = \left[\begin{array}{cc} 2U'(y) & 0 \end{array}\right]. \end{aligned} \tag{F}$$

Here, $U(y) = \{y,$ Couette flow; $1 - y^2,$ Poiseuille flow$\}$, $U'(y) = \mathrm{d}U(y)/\mathrm{d}y$, and $\boldsymbol{\Delta}^2 = \partial_{yyyy} - 2k_z^2\partial_{yy} + k_z^4$ with both Dirichlet and Neumann boundary conditions.

A system of equations (2) is in the form suitable for analysis performed in § IV where an explicit characterization of the Reynolds number dependence for the components of the frequency response of (1) is provided. It is noteworthy that for 2D/3C model there is no coupling from $\phi_5 = \tau_{xx}$ to the equations for the other flow-field components in (2); in particular, this demonstrates that evolution of τ_{xx} in 2D/3C model does not influence evolution of u, v, and w. We also note a one way coupling from Eqs. (2a) and (2b) to Eqs. (2c) and (2d); this indicates that the dynamical properties of $\phi_3 = \omega_y$ and $\boldsymbol{\phi}_4 = \left[\begin{array}{cc} \tau_{xy} & \tau_{xz} \end{array}\right]^T$ are influenced by $\phi_1 = v$ and $\boldsymbol{\phi}_2 = \left[\begin{array}{ccc} \tau_{yy} & \tau_{yz} & \tau_{zz} \end{array}\right]^T$ but not vice-versa.

III. Frequency responses for streamwise constant perturbations

The frequency response represents a cornerstone of the input-output analysis of linear dynamical systems [6]. A utility of input-output analysis in understanding early stages of transition in wall-bounded shear flows of Newtonian fluids is by now well documented; we refer the reader to a recent review article [2] for more information. It turns out that input-output approach also reveals important facets of transitional dynamics in channel flows of viscoelastic fluids [3].

To provide a self-contained treatment, we next present a brief summary of a notion of the spatio-temporal frequency response of streamwise constant equations with forcing; we

invite the reader to see [7] for additional details. The spatio-temporal frequency response of system (1) is given by

$$\mathbf{H}(k_z,\omega) \;=\; \mathbf{C}(k_z)(\mathrm{i}\omega\mathbf{I}-\mathbf{A}(k_z))^{-1}\bar{\mathbf{B}}(k_z),$$

where ω denotes the temporal frequency. The frequency response is obtained directly from the Fourier symbols of the operators in (1), and for any pair (k_z,ω) it represents an operator (in y) that maps the forcing field into the velocity field.

The frequency response of a system with a stable generator $\mathbf{A}$ describes the steady-state response to harmonic input signals across temporal and spatial frequencies. Since $\mathbf{H}$ is an operator valued function of two independent variables (k_z,ω), there is a variety of ways to visualize its properties. In this paper, we study the Hilbert–Schmidt norm of $\mathbf{H}$

$$||\mathbf{H}(k_z,\omega)||^2_{HS} \;=\; \mathrm{trace}\left(\mathbf{H}^*(k_z,\omega)\mathbf{H}(k_z,\omega)\right),$$

where $\mathbf{H}^*$ represents adjoint of operator $\mathbf{H}$. For any pair (k_z,ω), the Hilbert–Schmidt norm quantifies the power spectral density of the velocity field in the 2D/3C model subject to harmonic (in z) white, unit variance, temporally stationary, stochastic (in y and t) body forcing. Furthermore, the temporal-average of the power spectral density of $\mathbf{H}$ yields the H_2 norm of system (1) [6]

$$\left[\|\mathbf{H}\|_2^2\right](k_z) \;=\; \frac{1}{2\pi}\int_{-\infty}^{\infty}||\mathbf{H}(k_z,\omega)||^2_{HS}\,\mathrm{d}\omega.$$

The frequency responses of viscoelastic channel flows (as a function of k_x and k_z) are quantified in [3] in terms of the H_2 norm. We note that at any k_z, the H_2 norm determines the energy (variance) amplification of harmonic (in z) stochastic (in y and t) disturbances [7], [8].

We finally note that the frequency response of system (1), $\mathbf{v}=\mathbf{H}\mathbf{d}$, has the following 3×3 block-decomposition:

$$\begin{bmatrix} u\\ v\\ w\end{bmatrix} = \begin{bmatrix} \mathbf{H}_{u1} & \mathbf{H}_{u2} & \mathbf{H}_{u3}\\ \mathbf{H}_{v1} & \mathbf{H}_{v2} & \mathbf{H}_{v3}\\ \mathbf{H}_{w1} & \mathbf{H}_{w2} & \mathbf{H}_{w3}\end{bmatrix}\begin{bmatrix} d_1\\ d_2\\ d_3\end{bmatrix}, \qquad \text{(FR)}$$

which is suitable for uncovering the effectiveness (energy content) of forcing (velocity) components. In this representation, $\mathbf{H}_{rj}(k_z,\omega;Re,\beta,\mu)$ denotes the frequency response operator from d_j to r, with $\{j=1,2,3;\ r=u,v,w\}$. Our notation suggests that – in addition to the spanwise wavenumber k_z and the temporal frequency ω – each component of $\mathbf{H}$ also depends on the Reynolds number Re, the viscosity ratio β, and the elasticity number μ.

IV. Dependence of frequency responses on the Reynolds number

In this section, we study how the power spectral densities and the steady-state energy densities scale with Re for each of the components of the frequency response (FR). Furthermore, the square-additive property of these two quantities is used to determine the aggregate effect of forces in all three spatial directions $\mathbf{d}$ on all three velocity components $\mathbf{v}$. We analytically establish that the frequency responses from both wall-normal and spanwise forces to streamwise velocity scale as Re^2, while the frequency responses of all other components in Eq. (FR) scale at most as Re. This extends the Newtonian-fluid results [7] to channel flows of Oldroyd-B fluids.

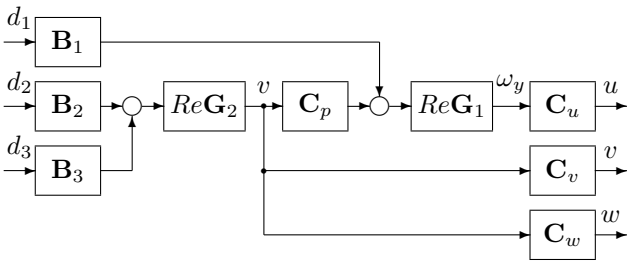

Fig. 1. Block diagram representation of the linearized 2D/3C model.

Application of the temporal Fourier transform to Eq. (2) facilitates elimination of polymer stresses from the 2D/3C model. This leads to an equivalent representation of system (2) in terms of its block diagram, which is shown in Fig. 1. From this block diagram, it follows that operator $\mathbf{H}(k_z,\omega;Re,\beta,\mu)$ in (FR) can be expressed as

$$\begin{bmatrix} u\\ v\\ w\end{bmatrix} = \begin{bmatrix} Re\,\bar{\mathbf{H}}_{u1} & Re^2\,\bar{\mathbf{H}}_{u2} & Re^2\,\bar{\mathbf{H}}_{u3}\\ 0 & Re\,\bar{\mathbf{H}}_{v2} & Re\,\bar{\mathbf{H}}_{v3}\\ 0 & Re\,\bar{\mathbf{H}}_{w2} & Re\,\bar{\mathbf{H}}_{w3}\end{bmatrix}\begin{bmatrix} d_1\\ d_2\\ d_3\end{bmatrix}, \quad (3)$$

with the Re-independent operators $\bar{\mathbf{H}}(k_z,\Omega;\beta,\mu)$: $\{\bar{\mathbf{H}}_{u1}=\mathbf{C}_u\mathbf{G}_1\mathbf{B}_1;\ \bar{\mathbf{H}}_{uj}=\mathbf{C}_u\mathbf{G}_1\mathbf{C}_p\mathbf{G}_2\mathbf{B}_j,\ j=2,3;\ \bar{\mathbf{H}}_{rj}=\mathbf{C}_r\mathbf{G}_2\mathbf{B}_j,\ r=v,w,\ j=2,3;\ \mathbf{G}_1=(\mathrm{i}\Omega\mathbf{I}-\mathbf{S})^{-1};\ \mathbf{G}_2=(\mathrm{i}\Omega\mathbf{I}-\mathbf{L})^{-1}\}$, and $\Omega=\omega Re$. On the other hand, operators $\mathbf{L}$, $\mathbf{S}$, and $\mathbf{C}_p$ are defined by:

$$\mathbf{L} \;=\; \frac{1+\mathrm{i}\beta\mu\Omega}{1+\mathrm{i}\mu\Omega}\boldsymbol{\Delta}^{-1}\boldsymbol{\Delta}^2,\quad \mathbf{S} \;=\; \frac{1+\mathrm{i}\beta\mu\Omega}{1+\mathrm{i}\mu\Omega}\boldsymbol{\Delta},$$
$$\mathbf{C}_p \;=\; \mathbf{C}_{p1}+\frac{\mu}{(1+\mathrm{i}\mu\Omega)^2}\mathbf{C}_{p2},\quad \mathbf{C}_{p1} \;=\; -\mathrm{i}k_zU'(y),$$
$$\mathbf{C}_{p2} \;=\; \mathrm{i}k_z(1-\beta)\left(U'(y)\boldsymbol{\Delta}+2U''(y)\partial_y\right).$$

In the limit $\beta\to 1$, these operators simplify to the Orr-Sommerfeld ($\boldsymbol{\Delta}^{-1}\boldsymbol{\Delta}^2$), Squire ($\boldsymbol{\Delta}$), and coupling ($-\mathrm{i}k_zU'(y)$) operators in streamwise constant flows of Newtonian fluids with $Re=1$. We note that even though viscoelastic effects modify some of the operators in Fig. 1, there is a striking similarity between block-diagram representations of the 2D/3C models of non-Newtonian and Newtonian fluids [7]. In particular, Fig. 1 shows that the frequency responses from d_2 and d_3 to u scale as Re^2, whereas the responses from all other forcing components to other velocity components scale linearly with Re. It should be noted that the frequency responses of streamwise constant Newtonian fluids show same scaling with Re [7]. The coupling operator, $\mathbf{C}_p$, is crucial for the Re^2-scaling. In Newtonian fluids $\mathbf{C}_p$ corresponds to the vortex tilting term, $\mathbf{C}_{p1}$; in viscoelastic fluids $\mathbf{C}_p$ also contains an additional term, $\mathbf{C}_{p2}$, that captures the coupling from the wall-normal velocity to the wall-normal vorticity due to the work done by the polymer on the flow. In the absence of the coupling operator, all the components of $\mathbf{H}(\omega,k_z;Re,\beta,\mu)$ scale at most linearly with Re. Fig. 1 also suggests that – for the 2D/3C model – streamwise forcing does not influence the wall-normal and spanwise velocities which is in agreement with Newtonian fluids results [7].

The following theorem follows directly from (3) and the definition of the Hilbert-Schmidt norm.

Theorem 1: For streamwise constant Poiseuille and Couette flows of Oldroyd-B fluids, the Hilbert–Schmidt norms of operators $\mathbf{H}_{rj}(k_z,\omega;Re,\beta,\mu)$ that map d_j into r, $\{r = u,v,w;\ j=1,2,3\}$, are given by

$$\begin{bmatrix} ||\mathbf{H}_{u1}||^2_{HS} & ||\mathbf{H}_{u2}||^2_{HS} & ||\mathbf{H}_{u3}||^2_{HS} \\ ||\mathbf{H}_{v1}||^2_{HS} & ||\mathbf{H}_{v2}||^2_{HS} & ||\mathbf{H}_{v3}||^2_{HS} \\ ||\mathbf{H}_{w1}||^2_{HS} & ||\mathbf{H}_{w2}||^2_{HS} & ||\mathbf{H}_{w3}||^2_{HS} \end{bmatrix} = \begin{bmatrix} l_{u1}Re^2 & m_{u2}Re^4 & m_{u3}Re^4 \\ 0 & l_{v2}Re^2 & l_{v3}Re^2 \\ 0 & l_{w2}Re^2 & l_{w3}Re^2 \end{bmatrix}$$

where $l_{rj}(k_z,\Omega;\beta,\mu)$ and $m_{rj}(k_z,\Omega;\beta,\mu)$ are functions independent of Re, and $\Omega := \omega Re$. Furthermore, the Hilbert–Schmidt norm of operator $\mathbf{H}$, $\mathbf{v} = \mathbf{Hd}$, is given by $||\mathbf{H}(k_z,\omega;Re,\beta,\mu)||^2_{HS} = l(k_z,\Omega;\beta,\mu)Re^2 + m(k_z,\Omega;\beta,\mu)Re^4$, where $l = l_{u1}+l_{v2}+l_{v3}+l_{w2}+l_{w3}$ and $m = m_{u2}+m_{u3}$.

Several important observations follow from Theorem 1 without doing any detailed computations. First, the power spectral densities of operators $\mathbf{H}_{u2}$ and $\mathbf{H}_{u3}$ scale as Re^4; in all other cases they scale at most as Re^2. This illustrates the dominance of the streamwise velocity perturbations and the forces in the wall-normal and spanwise directions in high-Reynolds-number channel flows of streamwise constant Oldroyd-B fluids. Second, apart from $||\mathbf{H}_{u2}||^2_{HS}$ and $||\mathbf{H}_{u3}||^2_{HS}$, the other power spectral densities in Theorem 1 do not depend on the base velocity and stresses. These two power spectral densities depend on the coupling operator, $\mathbf{C}_p$, and thus their values differ in Poiseuille and Couette flows. Third, functions $l_{rj}(k_z,\Omega;\beta,\mu)$ and $m_{rj}(k_z,\Omega;\beta,\mu)$ do not depend on the Reynolds number. Thus, Re only affects the magnitudes of $||\mathbf{H}_{rj}||^2_{HS}$, and regions of temporal frequencies ω where these power spectral densities peak. As Re increases, these ω-regions shrink as $1/Re$.

We next exploit the above results to establish the Re-dependence of the H_2 norm for different components of frequency response operator (FR). For example, $\left[||\mathbf{H}_{u2}||^2_2\right](k_z;Re,\beta,\mu)$ is determined by

$$\begin{aligned} ||\mathbf{H}_{u2}||^2_2 &= \frac{1}{2\pi}\int_{-\infty}^{\infty} ||\mathbf{H}_{u2}(\omega,k_z;Re,\beta,\mu)||^2_{HS}\,\mathrm{d}\omega \\ &= \frac{Re^4}{2\pi}\int_{-\infty}^{\infty} ||\bar{\mathbf{H}}_{u2}(\Omega,k_z;\beta,\mu)||^2_{HS}\,\mathrm{d}\omega \\ &= \frac{Re^3}{2\pi}\int_{-\infty}^{\infty} ||\bar{\mathbf{H}}_{u2}(\Omega,k_z;\beta,\mu)||^2_{HS}\,\mathrm{d}\Omega \\ &=: Re^3 g_{u2}(k_z;\beta,\mu). \end{aligned}$$

Similar procedure can be used to determine the H_2 norms of all other components of operator $\mathbf{H}$ in (FR), which proves Corollary 2.

Corollary 2: For streamwise constant Poiseuille and Couette flows of Oldroyd-B fluids, the H_2 norms of operators $\mathbf{H}_{rj}(k_z,\omega;Re,\beta,\mu)$ that map d_j into r, $\{r = u,v,w;\ j = 1,2,3\}$, are given by

$$\begin{bmatrix} ||\mathbf{H}_{u1}||^2_2 & ||\mathbf{H}_{u2}||^2_2 & ||\mathbf{H}_{u3}||^2_2 \\ ||\mathbf{H}_{v1}||^2_2 & ||\mathbf{H}_{v2}||^2_2 & ||\mathbf{H}_{v3}||^2_2 \\ ||\mathbf{H}_{w1}||^2_2 & ||\mathbf{H}_{w2}||^2_2 & ||\mathbf{H}_{w3}||^2_2 \end{bmatrix} = \begin{bmatrix} f_{u1}Re & g_{u2}Re^3 & g_{u3}Re^3 \\ 0 & f_{v2}Re & f_{v3}Re \\ 0 & f_{w2}Re & f_{w3}Re \end{bmatrix},$$

where $f_{rj}(k_z;\beta,\mu)$ and $g_{rj}(k_z;\beta,\mu)$ are functions independent of Re. Furthermore, the H_2 norm of operator $\mathbf{H}$, $\mathbf{v} = \mathbf{Hd}$, is given by $\left[||\mathbf{H}||^2_2\right](k_z;Re,\beta,\mu) = f(k_z;\beta,\mu)Re + g(k_z;\beta,\mu)Re^3$, where $f = f_{u1}+f_{v2}+f_{v3}+f_{w2}+f_{w3}$ and $g = g_{u2}+g_{u3}$.

V. Parametric study of power spectral densities

In § IV, we derived an explicit dependence for each component of the frequency response operator (FR) on Re. Here, we investigate the effect of β and μ on the (Ω, k_z)-parameterized plots of power spectral densities $\|\mathbf{H}_{rj}\|^2_{HS}$, $\{r = u,v,w;\ j = 1,2,3\}$, by setting $Re = 1$ in Theorem 1. In all the plots presented in this section, 100×90 logarithmically-spaced grid points are used in the (Ω,k_z)-plane. The temporal frequency and spanwise wavenumber are varied between 0.01 and 25.11 (Ω) and 0.1 and 15.84 (k_z), respectively. The components of $\left[\|\bar{\mathbf{H}}_{rj}\|^2_{HS}\right](k_z,\Omega;\beta,\mu)$ are computed using the method developed in [9].

Figures 2 and 3, respectively, show the (Ω,k_z)-dependence of the Re-independent functions l_{rj} and m_{rj} in Theorem 1, for $\beta = 0.1$ and $\mu = 10$. We note that the l-functions are nominal flow independent and only the m-functions depend on nominal velocity and polymer stresses. (The results in Fig. 3 are computed in Couette flow.) Since in 2D/3C model, d_1 does not affect v and w, we do not plot l_{v1} and l_{w1} in Fig. 2. Also, since $l_{w2} = l_{v3}$, we only plot $l_{v3}(k_z,\Omega;\beta,\mu)$. The important observations are:

Several frequency response components peak at non-zero Ω. This is in contrast to Newtonian fluids, where all power spectral densities attain their maxima at $\Omega = 0$ [9]. Also, since the peaks for different components of the frequency response are observed at different locations in the (Ω,k_z)-plane, these plots uncover distinct amplification mechanisms. It is worth mentioning that the locations of the peaks shift depending upon β and μ values. Our results indicate that viscoelastic effects introduce additional timescales which promotes development of spatio-temporal flow patterns with smaller time constants than in Newtonian fluids.

At low Re values (≤ 1)*, depending upon* μ*, either input-output amplification from* d_1 *to* u *attains the largest value or the amplification from* (d_2,d_3) *to* u *attains the largest value.* At small values of μ, l_{u1} has the largest magnitude; this suggests that at small Reynolds numbers and small elasticity numbers the streamwise forcing has the strongest influence (on the velocity) and the most powerful impact of this forcing is on the streamwise velocity component. At higher values of μ, m_{u2} and m_{u3} in Theorem 1 achieve the largest magnitudes; this suggests that at higher elasticity numbers the spanwise and wall-normal forces have the strongest influence (on the velocity) and that the streamwise velocity component is most energetic.

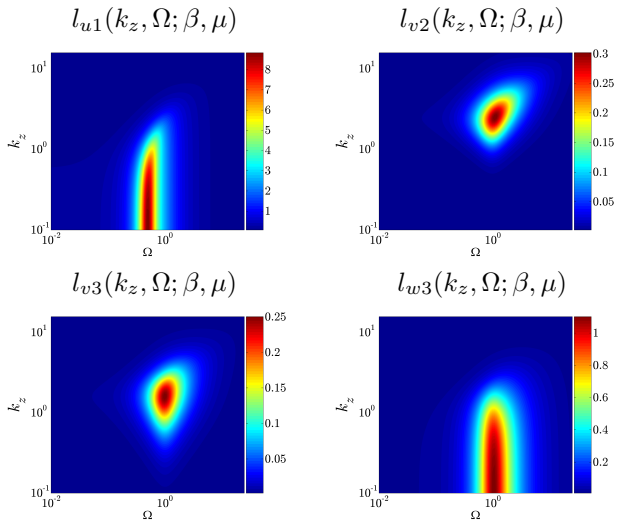

Fig. 2. Plots of l-functions in Theorem 1 for $\beta = 0.1$, $\mu = 10$.

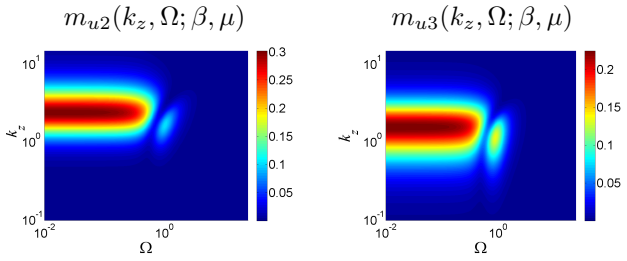

Fig. 3. Plots of m-functions in Theorem 1 in Couette flow with $\beta = 0.1$, $\mu = 10$.

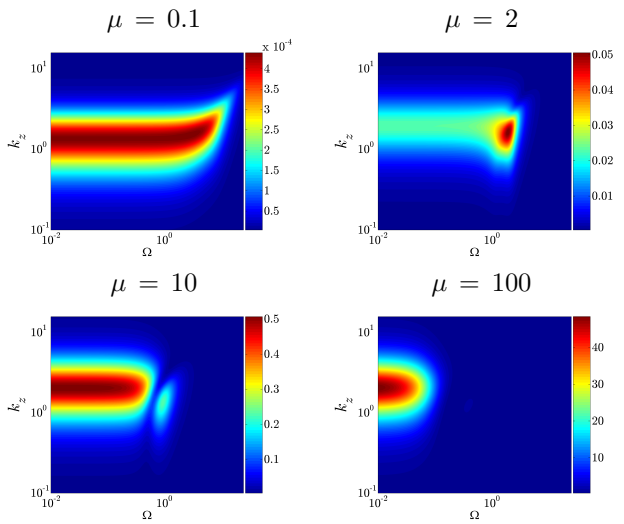

Fig. 4. Plots of function $m(k_z,\Omega;\beta,\mu)$ in Theorem 1 in Couette flow with $\beta = 0.1$, $\mu = \{0.1, 2, 10, 100\}$.

For the nominal flow independent functions l_{rj} in Theorem 1, a very good analytical estimate for $\Omega_{\max}$ (the value of Ω corresponding to the maxima of functions l_{rj}) can be determined by projecting the operators in $\mathbf{H}_{rj}$ on the first eigenfunctions of $\mathbf{\Delta}^{-1}\mathbf{\Delta}^2$ (for l_{rj}, $\{r = v, w;\ j = 2, 3\}$) and $\mathbf{\Delta}$ (for l_{u1}). (We refer the reader to Appendix B of [7] for spectral analysis of these two operators in 2D/3C model.) Using this approach, we determine the following expression for $\Omega_{\max}$: $\{(1/\mu)(\sqrt{\mu|\lambda_1(k_z)|(1-\beta)(\mu|\lambda_1(k_z)|(1+\beta)+2)}-1)^{1/2}$, $\mu > (\sqrt{2/(1-\beta)}-1)/(|\lambda_1(k_z)|(1+\beta))$; 0, otherwise$\}$ where $\lambda_1(k_z)$ is the principal eigenvalue of the underlying operator ($\mathbf{\Delta}$ for l_{u1}; $\mathbf{\Delta}^{-1}\mathbf{\Delta}^2$ for l_{rj}, $\{r = v, w;\ j = 2, 3\}$). From this expression it follows that $\Omega_{\max}$ increases with a decrease in β and that it exhibits a maximum in μ. Furthermore, for $\mu \gg 1$, $\Omega_{\max}$ approximately scales as $1/\sqrt{\mu}$, suggesting a slow rate of decay of $\Omega_{\max}$ with μ for large elasticity numbers.

The analytical expressions for $\Omega_{\max}$ are much more difficult to obtain for the nominal flow dependent functions m in Theorem 1. In spite of this, essential trends can be ascertained from Fig. 4 which shows the plots of function $m(k_z,\Omega;\beta,\mu)$ in Couette flow with $\beta = 0.1$ and $\mu = \{0.1, 2, 10, 100\}$. This function quantifies the power spectral density of the frequency response operator that maps (d_2, d_3) to streamwise velocity u at $Re = 1$. For $\mu = 0.1$, the frequency response achieves global maximum at $\Omega_{\max} = 0$, but the broad spectrum in Ω around $k_z \approx O(1)$ indicates that the large values are maintained up until $\Omega \approx 5$. On the other hand, at $\mu = 2$, the global peak is located in the narrow region around $\Omega_{\max} \approx 2$. With a further increase in elasticity number, two competing peaks at zero and $O(1)$ temporal frequencies appear; finally, for large values of μ the spectrum peaks shifts to the narrow region around zero temporal frequency, with $\Omega_{\max} = 0$.

VI. Parametric Study of Energy Amplification

In this section, we study the effect of β and μ on the k_z-parameterized plots of $\|\mathbf{H}\|_2^2$, by setting $Re = 1$ in Corollary 2. Functions f and g in Corollary 2 are obtained from the solutions of appropriate Lyapunov equations. For numerical approximation, we use Chebyshev collocation technique [10]; between 30 and 50 collocation points in y were found to be sufficient to obtain accurate results.

Corollary 2 suggests that at higher Re values, g is expected to contribute most to energy amplification, whereas at smaller Re values, f is expected to contribute most to energy amplification; we will show that the latter observation holds only at moderate values of μ. Furthermore, from Corollary 2, it follows that only streamwise velocity contributes to function g; this contribution arises due to amplification from d_2 and d_3 to u. On the other hand, amplification from d_1 to u and (d_2, d_3) to (v, w) is captured by function f. We note that f is the same for all channel flows and only g depends on the underlying nominal flow; for further analysis of function g, we restrict our attention to Couette flow. All plots in this section are given in the log-log scale.

Figures 5 and 6 show $f(k_z)$ and $g(k_z)$ at different β and μ values. We note that the magnitudes of both f and g increase with an increase in μ and a decrease in β. This indicate that energy amplification becomes weaker as one approaches Newtonian fluid limit. Furthermore, in all the cases, f monotonically decreases with k_z, while g achieves a maximum at $O(1)$ values of k_z. This suggests that the contribution from g is responsible for the energy density peaks observed at higher Reynolds numbers [3], confirming our earlier claim that at higher Re, $\|\mathbf{H}\|_2^2 \approx gRe^3$.

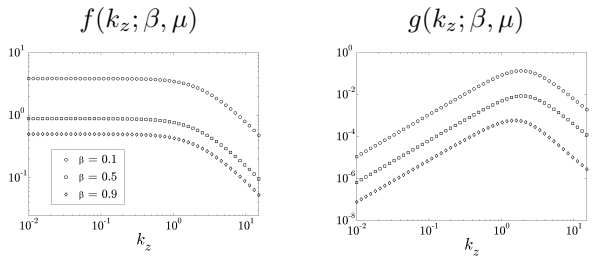

Fig. 5. Variation in f and g with k_z for $\mu = 10$ and $\beta = \{0.1, 0.5, 0.9\}$; g in Couette flow is shown.

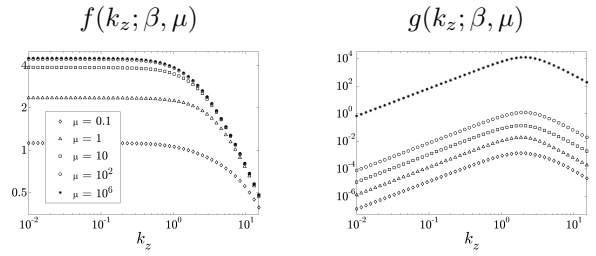

Fig. 6. Variation in f and g with k_z for $\beta = 0.1$ and $\mu = \{0.1, 1, 10, 10^2, 10^6\}$; g in Couette flow is shown.

Plots in Fig. 6 suggest that g increases monotonically with μ, while f reaches a saturation limit for sufficiently large values of μ. Thus, even in low inertial regimes, contribution of g to the energy density can be significant if elasticity number, μ, is large enough. In particular, this demonstrates that energy density peaks observed in [3] at $\{k_x = 0,\ Re = 0.1,\ \beta = 0.1,\ \mu = 10^6\}$ arise due to the contribution of E_2.

Figure 7 shows the k_z-dependence of $g(k_z;\beta,\mu)/\mu$ in Couette flow with $\beta = 0.1$ for five different values of elasticity number, $\mu = \{0.1, 1, 10, 10^2, 10^6\}$. It is evident that the five curves almost collapse on each other. This is a remarkable discovery in view of rather complicated dependence of the underlying equations on μ and the range of elasticity numbers considered. Our ongoing theoretical effort is directed towards development of an explicit scaling of f and g with μ; we conjecture that for large enough values of elasticity number f approximately becomes μ-independent, while g approximately scales linearly with μ. This would suggest the following approximate scaling of the energy amplification with elasticity number for $\mu \gg 1$, $\left[\|\mathbf{H}\|_2^2\right](k_z;Re,\beta,\mu) \approx Re\tilde{f}(k_z;\beta) + \mu Re^3\tilde{g}(k_z;\beta)$, where $\tilde{f}$ and $\tilde{g}$ are μ-independent functions. If this scaling turns out to be correct, our results would indicate an interesting interplay between inertial and viscoelastic effects in energy amplification of Oldroyd-B fluids with low Reynolds/high elasticity numbers [11], [12].

VII. Concluding remarks

The effects of streamwise constant 3D perturbations on the behavior of viscoelastic fluids are investigated using an input-output analysis, where the components of frequency response operator are analyzed. This study supplements a previous study by the authors [3], where the aggregate effect of disturbances was examined, and helps in understanding the relative importance of the disturbances on the different velocity components. In this study, we consider streamwise constant perturbations as they are most amplified by the linearized dynamics. We present the explicit scaling of the components of frequency response with Reynolds number. At higher Reynolds numbers, the forces in the wall-normal and spanwise directions have the strongest influence on the flow field and the impact of these forces is largest on the streamwise velocity. At lower Reynolds numbers, the streamwise force is the most dominant and it affects the streamwise velocity the most. In some of the cases, the components of frequency response peak at non-zero frequencies. This is distinct from Newtonian fluids behavior, where peaks are always observed at zero frequency, suggesting that elasticity introduces additional timescales and promotes development of flow patterns with smaller time constants than in Newtonian fluids. We found that the temporal frequencies, corresponding to the peaks in the components of frequency response, decrease with an increase in viscosity ratio and show maximum in the elasticity number. One of the most notable findings of this paper is the observation that elasticity can produce considerable energy amplification even when inertial effects are weak; this amplification may then serve as a route through which channel flows of viscoelastic fluids transition to turbulence at low Reynolds numbers [11], [12].

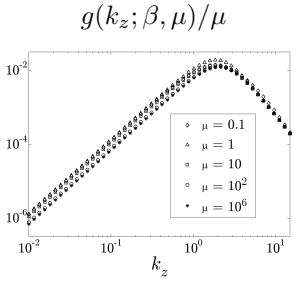

Fig. 7. The k_z-dependence of g/μ in Couette flow with $\beta = 0.1$, $\mu = \{0.1, 1, 10, 10^2, 10^6\}$.

References

[1] A. N. Morozov and W. Saarloos, "Subcritical finite-amplitude solutions for plane Couette flow of viscoelastic fluids," *Phys. Rev. Lett.*, vol. 95, pp. 024 501–1–024 501–4, 2005.

[2] P. J. Schmid, "Nonmodal stability theory," *Ann. Rev. Fluid Mech.*, vol. 39, pp. 129–162, 2007.

[3] N. Hoda, M. R. Jovanović, and S. Kumar, "Energy amplification in channel flows of viscoelastic fluids," *J. Fluid. Mech.*, vol. 601, pp. 407–424, 2008.

[4] R. G. Larson, *The Structure and Rheology of Complex Fluids*. Oxford University Press, New York, 1999.

[5] W. C. Reynolds and S. C. Kassinos, "One-point modeling of rapidly deformed homogeneous turbulence," *Proceedings: Mathematical and Physical Sciences*, vol. 451, no. 1941, pp. 87–104, 1995.

[6] K. Zhou, J. C. Doyle, and K. Glover, *Robust and Optimal Control*. Prentice Hall, New Jersey, 1996.

[7] M. R. Jovanović and B. Bamieh, "Componentwise energy amplification in channel flows," *J. Fluid Mech.*, vol. 534, pp. 145–183, 2005.

[8] B. Bamieh and M. Dahleh, "Energy amplification in channel flows with stochastic excitations," *Phys. Fluids*, vol. 13, pp. 3258–3269, 2001.

[9] M. R. Jovanović and B. Bamieh, "A formula for frequency responses of distributed systems with one spatial variable," *Systems and Control Letters*, vol. 55, pp. 27–37, 2006.

[10] J. A. C. Weideman and S. C. Reddy, "A MATLAB differentiation matrix suite," *ACM transaction of mathematical software*, vol. 26, no. 4, pp. 465–519, 2000.

[11] R. G. Larson, "Turbulence without inertia," *Nature*, vol. 405, pp. 27–28, 2000.

[12] A. Groisman and V. Steinberg, "Elastic turbulence in a polymer solution flow," *Nature*, vol. 405, pp. 53–55, 2000.